Source process of the 2011 Tohoku great earthquake and following triggered events inferred from strong-motion records

Y. Shiba
Central Research Institute of Electric Power Industry, Japan

SUMMARY:

The source rupture process of the 2011 Tohoku M9.0 great earthquake and following induced earthquakes are inferred by the waveform inversion using the empirical Green's function. For the main shock the rupture scenario of the kind of multi-faulting is found to be appropriate in order to interpret two distinctive strong-motion packets with a long time interval. I further estimate the source models of two moderate earthquakes triggered by the main shock, which are the intra-slab earthquake of M 7.2 occurring off Miyagi prefecture beneath the deep end of the main-shock fault and the shallow inland earthquake of M 7.0 at Fukushima prefecture. The estimated source model of the off-Miyagi intra-slab earthquake consists of a single asperity with short rise time, suggesting high slip velocity and strong radiation of high-frequency motions. For the Fukushima inland earthquake the locations of estimated asperities are consistent with the measurement of the surface fault ruptures.

Keywords: 2011 Tohoku great earthquake, Triggered earthquake, Source process, Inversion, Strong motion

1. INTRODUCTION

The 2011 Tohoku great earthquake of Mw 9.0 was the largest event since the modern seismic observation by instruments had been carried out in Japan. Nearly 20 thousand people were killed or missed mainly by the huge tsunami generated along with this earthquake. The focal mechanism showing thrust type suggests that the main shock occurred in the plate boundary where the Pacific plate is subducting beneath the North American plate. Many aftershocks have been generated in the source area 500 km long and 200km wide as shown in Figure 1.1.

The Tohoku earthquake is also characterized as the event inducing several damaged earthquakes apart from the main-shock region. On April 7, about one month after the main shock occurrence (March 11), intra-slab earthquakes of Mj 7.2 occurred off the coast of Miyagi Prefecture, beneath the deep end of the main-shock fault. Four days after shallow inland earthquake of Mj 7.0 was generated near the coast (Hamadoori) of Fukushima Prefecture. The focal mechanism of the Hamadoori earthquake indicates the normal faulting and clear surface ruptures were recognized along two known active faults, Itozawa Fault and Yunodake Fault (i.e. Mizoguchi et al, 2012). Such a normal-fault event is considered to be triggered by the change of initial stress field after the large slippage on the main-shock fault plane. Figure 1.2 shows a schematic illustration of the faulting mechanisms for the March 11 Tohoku main shock, the April 7 off Miyagi intra-slab and the April 11 Hamadoori inland events. The epicenters of these two induced events are shown together in Figure 1.1.

In this article I estimate the slip distribution models for the main shock and two induced events introduced here by the waveform inversion method using the strong-motions records with the empirical Green's functions. Then the relationship between the seismic moment and other source parameters controlling the strong-motion generation on the seismic fault is verified in order to examine the scaling relation of the source parameters for the M 9 mega-earthquake and earthquakes

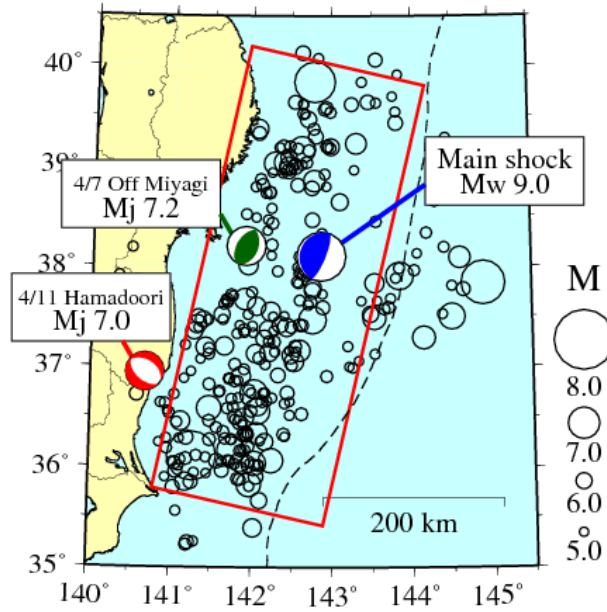occurring after the change of initial stress field in and around north-eastern Japan.

Figure 1.1 Epicenter of the Tohoku earthquake (Mw9.0) and aftershock distribution for three days after the main shock occurrence. A red rectangular indicates the estimated source area 500 km long and 200 km wide along the dipping fault plane. Epicentres of two induced events analyzed in this study are also shown with their focal mechanisms.
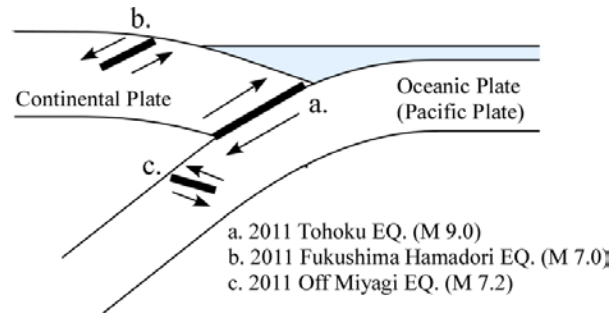

Figure 1.2 Schematic illustration of faulting mechanisms occurring at the subduction zone

2. SOURCE INVERSION METHOD

The inversion scheme used in this study is principally based on the method proposed by Shiba and Irikura (2005). This method is composed of the very fast simulated annealing (VFSA), which is one of the heuristic search algorithms used to statistically find the best global solution of a nonlinear nonconvex (multimodal) problem (Ingber, 1989), and the empirical Green's function method (EGFM; Irikura, 1986) as a forward process to calculate synthetic ground motions. The EGFM is a suitable method to evaluate high-frequency waveforms precisely since the subsurface structure modelling to estimate the path effect can be substituted by records of a small event. The search parameters are the moment density, rise rime and rupture time at each subfault divided according to the fault size of the element event used as an empirical Green's function. A Spatial smoothing constraint for the moment density and the rise time is imposed to suppress the instability of solutions, and suitable weights for the constraint are determined through minimizing ABIC (Akaike, 1980). On the other hand the rupture time variation obeys only the causality; that is, a subfault does not fail until its neighbour nearest to the rupture initiation point has failed.

However, as discussed after, the Tohoku earthquake was guessed to have shown very complicated rupture propagation on the fault plane. Thus I introduced a priori rupture scenario of the kind of multi-faulting for an analysis of the Tohoku earthquake.

3. ESTIMATED SOURCE MODELS

3.1. Fault plane models and empirical Green's functions

The configuration of assumed fault planes for the target events and the source parameters of the element events used as empirical Green's functions in the inversion procedure are shown in Table 3.1 and 3.2, resprctively. In general the subfault size is determined to correspond with the fault area of the element event derived from the corner frequency of the source spectrum. The source spectra for the element events were estimated from the observed records at the rock outcrops by removing the attenuation factors such as Q-values and site amplification factors based on the impedance ratio from the source to the receiver. The focal mechanisms of the target events were determined from the W-phase solution by USGS for the main shock and the moment tensor solution by F-net for the April 7 off Miyagi intra-slab event.

Table 3.1. Configuration of Assumed Fault Planes for the Target Events

Event	Length (km)	Width (km)	Strike (deg.)	Dip (deg.)
Tohoku EQ.	500	200	193	14
Off Miyagi EQ.	42	27	20	40
Hamadoori EQ. (Itozawa F.)	23.8	15.4	158	65
Hamadoori EQ. (Yunodake F.)	15.3	18.7	120	50

Table 3.2. Source Parameters of the Element Events Used as Empirical Green's Functions

Event	Origin Time	Focal Depth (km)	Mj	Fault Size (km^2)
Tohoku EQ.	2012/03/10 06:24	9.3	6.8	20×20
Off Miyagi EQ.	2011/04/28 06:45	53.4	4.8	1.5×1.5
Hamadoori EQ. (Itozawa F.)	2011/05/03 22:57	8.5	4.5	1.4×1.4
Hamadoori EQ. (Yunodake F.)	2011/04/11 22:05	11.3	4.7	1.7×1.7

For the April 11 Hamadoori inland earthquake two surface ruptures along with the known active faults, namely Itozawa and Yunodake faults, were observed after the event occurrence. The first motion solution by Hi-net operated by the National Research Institute for Earth Science and Disaster Prevention (NIED) corresponds with the geometry of the Itozawa fault, while the moment tensor solution by F-net (NIED) suggests similar fault mechanism with the Yunodake fault. Therefore in this study I assume two fault planes as the seismic source of the Hamadoori earthquake, whose strike angles agree with those of surface ruptures. The dip angle of the Yunodake fault is determined with reference to the F-net solution and that of the Itozawa fault is set up to cover the aftershock area in the depth range from 2 km to 16 km, which is coincident with the range of the seismogenic zone. The rupture is assumed to have started from the Itozawa fault and transferred to the Yunodake fault at the nearest point. Then the rupture on the Yunodake fault restarted with the circular propagation.

The magnitude of the element event for the Tohoku earthquake seems to be too large to use as an empirical Green's function. Since the fault length of the main shock extends to about 500 km, the station coverage for the source analysis should be expanded widely. Consequently it is necessary for the element event to have sufficiently large magnitude to maintain high signal to noise ratio in the observed waveform records at all stations. So it is noticed that the effect of heterogeneous faulting for the element event might be contained to the synthetic ground motions of the target event in the high frequency range.

3.2. Main shock –the Tohoku great earthquake- (Mw9.0)

Figure 3.1 shows the observed acceleration motions for the main shock at the near-fault stations on the rock outcrops operated by CRIEPI (RK-net; Shiba et al., 2009). The station CRIISM is installed at Ishinomaki city, Miyagi Prefecture, located 140 km west of the epicentre, and CRINME is the station at Fukushima Prefecture, about 100 km south from CRIISM. The acceleration waveform of CRIISM is composed of two distinct wave-packets appearing at intervals of 50 seconds. In the waveform observed at CRINME, more strong-motion phases with smaller durations are recognized, suggesting several small patch areas generating strong motions on the seismic fault near Fukushima Prefecture.
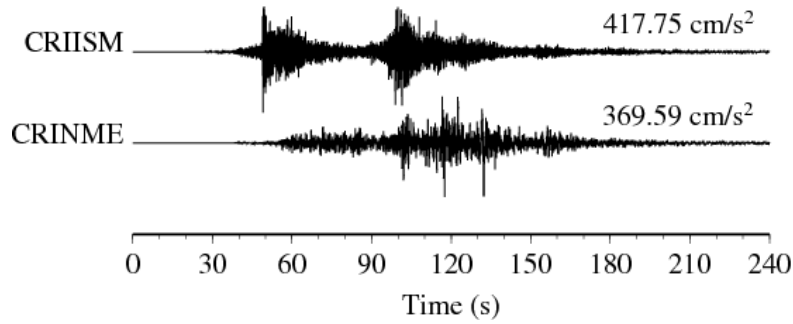

Figure 3.1 Acceleration motions of the 2011 Tohoku earthquake recorded at the near-source stations on rock outcrops operated by CRIEPI (EW-comp.). The locations of the stations are shown in Figure 3.3.

Since acceleration motions similar to that at CRIISM were observed at the stations in northern Tohoku district in common, these two wave packets are considered to have generated from the seismic source separately. Furthermore, they show very close apparent velocity, hence the strong-motion generation areas for these separated wave-packets are expected to be located close to each other. Because the inversion method in this study adopts the law of causality for the search of rupture times, it might not be possible to deduce such a complicated rupture process without any a priori assumptions. Therefore I introduced an additional assumption of the multi-faulting scenario for the main shock during the inversion procedure, that is, when the rupture front from the hypocenter reaches to the eastern edge on the fault plane near the trench, the rupture restarts toward the opposite, deeper side of the fault. Ide et al. (2011) proposed a similar scenario of fault rupture, due to the dynamic overshoot (excess reduction of the shear stress on the fault plane). Yagi and Fukahata (2011) pointed out a continuous slip with long duration at shallow area near the trench released roughly all of the accumulated elastic strain on the plate interface.

Shiba et al. (2012) estimated the moment density distribution as shown in Figure 3.2. Two horizontal velocity motions in the frequency range from 0.02 to 0.5 Hz (from 2 to 50 seconds) at 15 stations were used in the waveform inversion procedure. During the first rupture stage radiating from the hypocenter, the slip near the hypocenter is rather small. The areas of large moment release are the shallow plate boundary close to the Japan Trench and several deeper regions. Then the second rupture propagating from the trench axis eventually released the large moment in the vicinity of the hypocenter. The large moment-released areas (i.e. asperities) for the first and second rupture stages are complementary. At the CRIISM station the first strong motion arriving at 40 s in Figure 3.1 is considered to be radiated from the nearest asperity, and the second shaking at 90 s might come from the asperity near the hypocenter ruptured at the second stage. For the CRINME station nearby small asperities generated several strong-motion phases.

It should be noticed that one of the asperities during the main shock is coincident with the source area of the 1978 Off Miyagi earthquake of Mj7.4 (Wu et al., 2008) shown with a green rectangle in Figure 3.2. In the source region of the 1978 earthquake another event of Mj 7.2 occurred in 2005. Wu et al. (2008) indicates that the 2005 event ruptured the southern half of the source area of the 1978 event. Hence during the 2011 main shock the large moment was released from the remaining northern part of

the 1978 earthquake as shown in Figure 3.2. Total seismic moment is estimated to be 3.69×10^{22} Nm (Mw9.0) and the peak slip reaches 60m at the shallow area assuming a rigidity of 32 GPa.
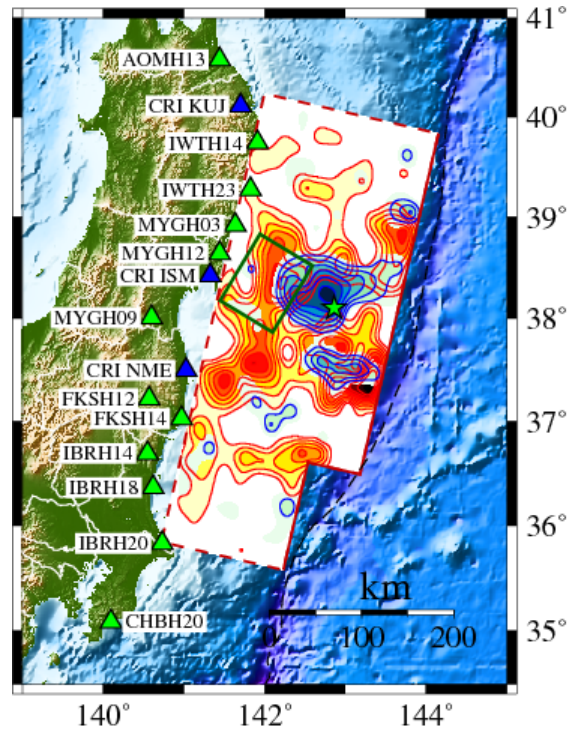

Figure 3.2 Map showing the moment density distribution of the 2011 Tohoku earthquake. Red contour shows the moment release at the first rupture stage and blue contour is that at the second stage. Observation stations used for the inversion analysis are shown with blue (RK-net) and green (KiK-net) triangles.

Figure 3.3 shows the snapshot of the moment release at intervals of 15 seconds. From 30 to 60 s at the asperity of the 1978 event the large moment is released, and from 60s the area in the vicinity of the hypocenter shows long slip for about 45 seconds. Another large moment release occurs at the asperities south of the 1978 event (off Fukushima Prefecture) from around 75 s.
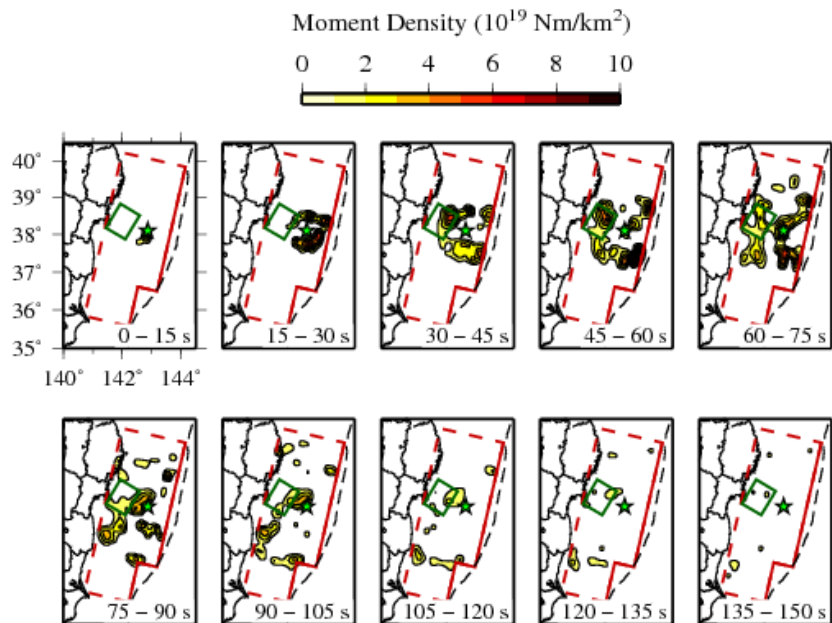

Figure 3.3 Snapshot of the moment release on the fault plane with 15 seconds interval
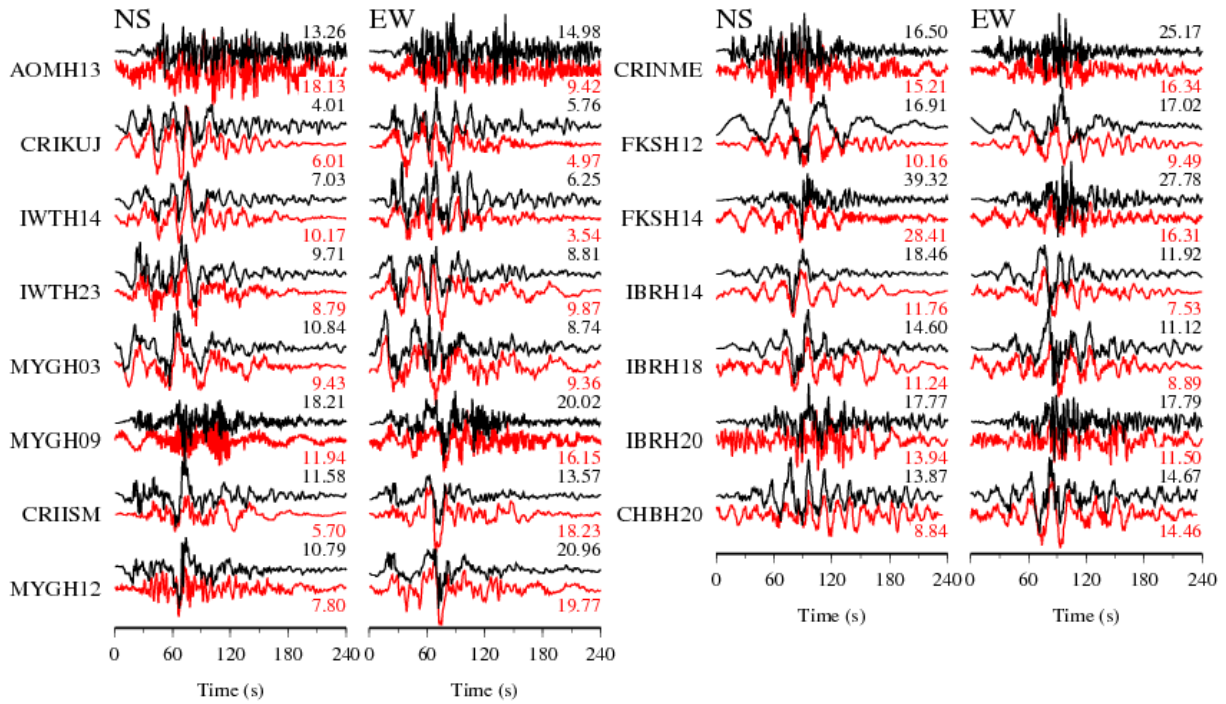
Figure 3.4 Comparison of synthetics (red) calculated from the source model with the observed data (black)

The comparison between the synthetic velocity motions calculated from the estimated source model and the observed data is shown in Figure 3.4. The waveform fit between them is mostly successful.

3.3. Off Miyagi intra-slab earthquake (Mj7.2)

The April 7 off Miyagi event of Mj7.2 was a down-dip compression type earthquake in the Pacific slab, estimated from the high dip angle in the moment tensor solution and the focal depth of 66 km. As shown in Figure 3.5, observed peak ground accelerations are much larger compared with the empirical attenuation relation by Si and Midorikawa (1999) particularly at closed distance. In Figure 3.6 I show the estimated moment slip distribution on the map (Shiba and Noguchi, 2012). The source model of the Off Miyagi earthquake is quite simple consisting of one asperity. The rupture started from the deep edge of the asperity and propagated up-dip toward the land (western direction), which might lead larger high-frequency motions at stations above the source area. In addition the rise time is found to be relatively short (Shiba and Noguchi, 2012), and it suggests high slip velocity and stress drop also generating large accelerations.
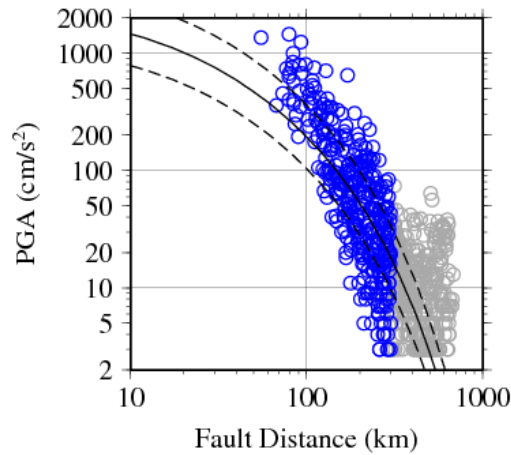

Figure 3.5 Comparison between the observed peak ground accelerations during the April 7 off Miyagi intra-slab earthquake and the empirical attenuation relation proposed by Si and Midorikawa (1999).
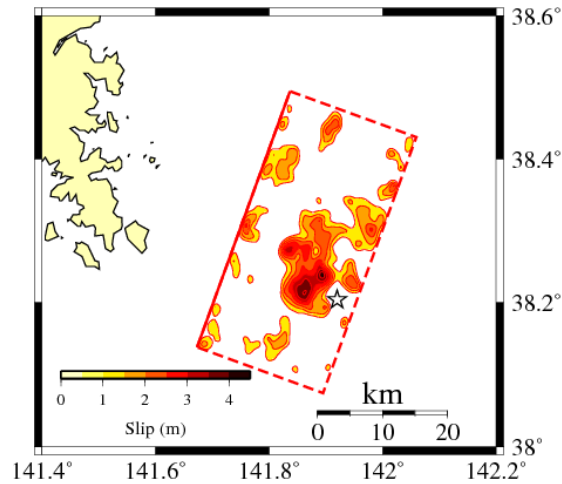
Figure 3.6 Map showing the slip distribution of the 2011 April 7 off Miyagi intra-slab earthquake

3.4. Hamadoori inland earthquake (Mj7.0)

The April 11 Hamadoori event of Mj7.0 is characterized as the normal faulting mechanism and two clear surface rupture zones along the known active faults as mentioned before. Assumed fault planes and station distribution for the inversion analysis are shown in Figure 3.7. As shown in the fault plane model, two fault planes cover almost aftershock area for 24 hours after the main shock. Since suitable aftershock records with similar source mechanism to the main-shock faults could not be obtained as shown in Figure 3.7, the difference of the radiation patterns between the target and element events was corrected following Boore and Boatwright (1984). The velocity motions in the frequency range up to 2 Hz were used for the inversion analysis.
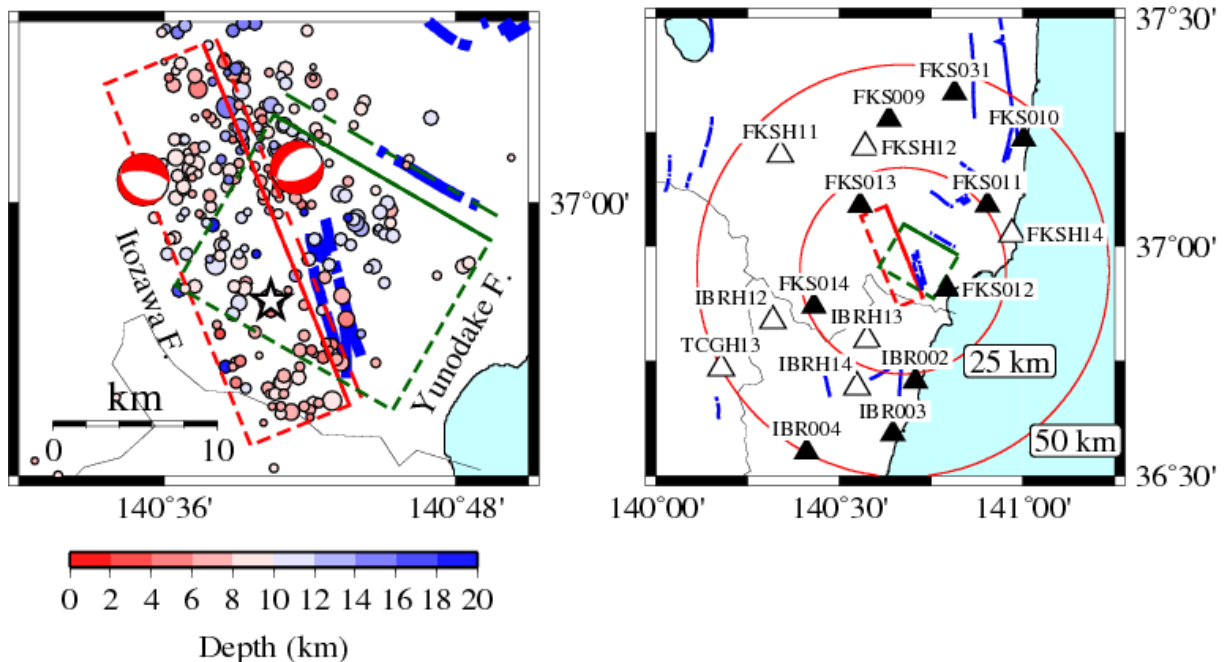

Figure 3.7 Fault plane model of the 2011 April 11 Hamadoori inland earthquake (right) and location map of observation stations (left). The right figure also shows the aftershock distribution for 24 hours after the main shock occurrence, together with the epicenters and focal mechanisms for the element events used as the empirical Green's functions.

The slip distribution model estimated by Shiba and Noguchi (2012) is shown in figure 3.8 with vertical offsets of the surface rupture measured by Mizoguchi et al. (2012). On the Itozawa fault the

large slip is located near the surface, while on the Yunodake Fault mainly two large slip areas are found close to the rupture transfer point from the Itozawa Fault and shallow part of the fault. For the Itozawa Fault few slips are generated near the transfer point. It might suggest the spatial change of the initial stress field to cause the rupture migration from the Itozawa to the Yunodake Fault. The estimated slip distribution during the Hamadoori earthquake is consistent with the measurement of the vertical offsets on the surface ruptures as shown in figure 3.8, which demonstrates the accuracy of the estimated source model.
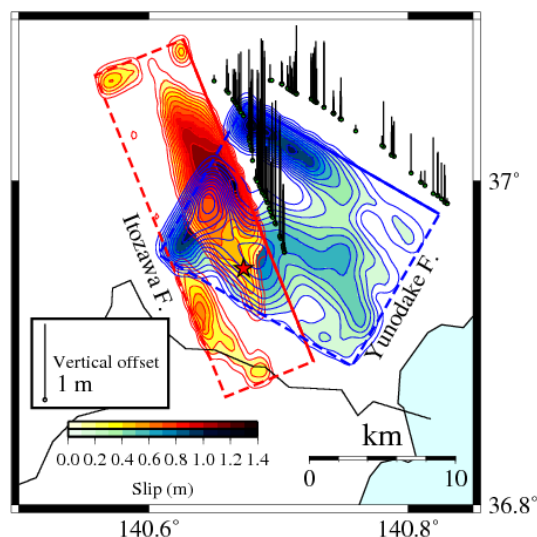

Figure 3.8 Map showing the slip distribution of the 2011 April 11 Hamadoori inland earthquake. The vertical offsets of the surface ruptures are also shown (Mizoguchi et al., 2012).

4. DISCUSSION

In order to improve the fault modelling for the evaluation of input ground motion used in the seismic design, it is important to examine the scaling relationships of the fault parameters controlling the strong motions, such as the asperity size, to the magnitude or the seismic moment based on the source process of the past earthquakes. Since the 2011 Tohoku earthquake was only the event of Mw 9.0 from which many strong-motion records near the source were obtained, it becomes possible to verify the scaling relations of the source parameters for the M 9 mega-earthquakes. Moreover it is also important to examine the scaling relations for the earthquakes of moderate size under the condition of partially extensional stress in the horizontal direction caused by large slips more than 50 m during the Tohoku earthquake. In particular the Hamadoori inland earthquake was one of the largest events with normal faulting in Japan. Therefore the knowledge concerning the scaling of the Hamadoori earthquake would be valuable information for the prediction of strong motions assuming the normal-fault event.

In this study I employ the objective criterion proposed by Somerville et al. (1999) to identify the rupture area and asperities from the slip distribution model derived by the source inversion procedure. Figure 4.1 shows the relationships of the rupture area and the combined area of asperities to the seismic moment respectively, for three events analyzed in this study. I adopt the seismic moment provided by F-net for two induced earthquake. Empirical scaling equations for inland crustal earthquakes (Somerville et al., 1999), inter-plate earthquakes (Murotani et al., 2008) and intra-slab earthquakes (Iwata and Asano, 2011) are also shown in the figure. For the events which occurred after the Tohoku main shock, the April 7 off Miyagi earthquake and the April 11 Hamadoori earthquake, estimated source parameters are roughly consistent with the empirical scaling relations. On the other hand both the rupture area and the combined asperity area of the Tohoku earthquake are less than half of the extrapolation of the empirical relationship proposed by Murotani et al. (2008). This result implies the relatively large slip occurred on the small fault plane area during the Tohoku earthquake.
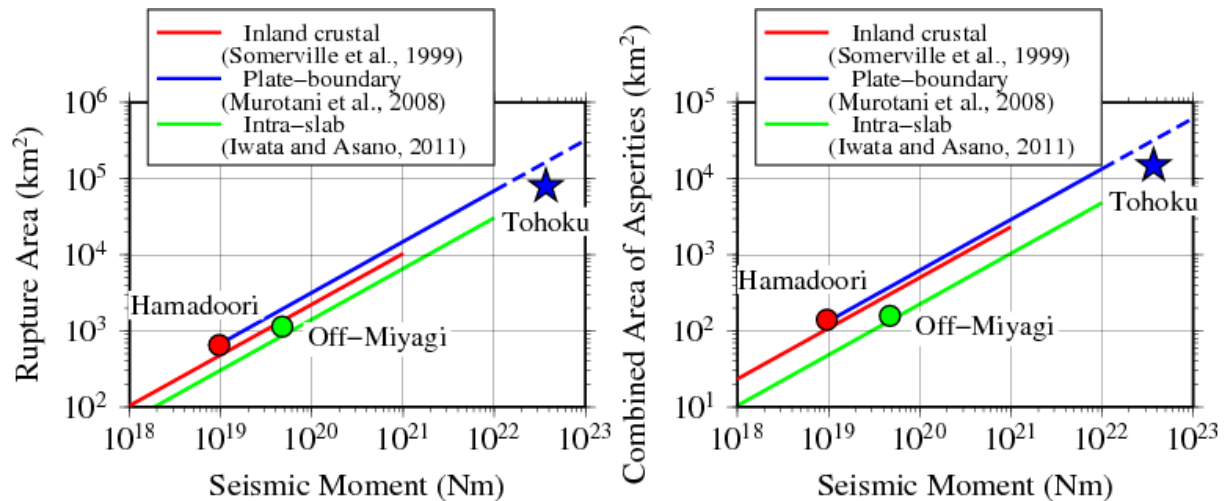
Figure 4.1.Scaling relations of the rupture area (left) and the combined asperity area (right) to the seismic moment for three events analyzed in this study

5. CONCLUSIONS

The source rupture process of the 2011 Tohoku Mw 9.0 great earthquake and following induced earthquakes are inferred by the waveform inversion using the empirical Green's function. For the Tohoku earthquake an additional assumption of the multi-faulting scenario was introduced during the inversion procedure to interpret the two distinct wave packets observed in the strong-motion records in common. The second rupture propagating from the trench axis released the large moment in the vicinity of the hypocenter. The locations of large asperities for the first and second rupture stages are complementary. The peak slip reaches 60m at the shallow plate boundary off the Miyagi and Fukushima Prefectures. The source model of the Off Miyagi intra-slab earthquake consists of one asperity and the rupture started from the deep edge of the asperity and propagated up-dip toward the land. And it might lead larger high-frequency motions at stations above the source area. For the Fukushima Hamadoori inland earthquake estimated slip distribution is consistent with the measurement of the vertical offsets on the surface ruptures. Finally the scaling relationships of fault parameters to the seismic moment are verified for these three events by comparing with the empirical equations. As a result the source parameters of two induced earthquakes correspond well with the empirical scaling relations, while the rupture area and the combined area of asperities of the Tohoku earthquake are rather small compared with the extrapolation of the empirical relationship, implying relatively large slip during the faulting process.

REFERENCES

Akaike, H. (1980). Likelihood and the Bayes procedure, Bayesian Statics, University Press, Valencia, Spain.
Boore, D. and Boatwright, J. (1984). Average body-wave radiation coefficients. *Bull. Seism. Soc. Am.* **74,** 1615-1621.
Ide, S., Baltay, A. and Beroza, G. C. (2011). Shallow dynamic overshoot and energetic deep rupture in the 2011 Mw 9.0 Tohoku-Oki Earthquake. *Science.* **332,** 1426, doi:10.1126/science.1207020.
Ingber, L. (1989). Very fast simulated re-annealing. *Mathl. Comput. Modelling*. **12**, 967-973.
Irikura, K. (1986). Prediction of strong acceleration motions using empirical Green's function. *Proc. 7th Japan Conf. Earthquake Engineering*. 151-156.

Iwata, T. and Asano, K. (2011). Characterization of the heterogeneous source model of intraslab earthquakes toward strong ground motion prediction. *Pure Appl. Geophys.* **168**, 117-124, doi: 10.1007/s00024-010-0128-7.

Mizoguchi, K., Uehara, S. and Ueta, K. (2012). Surface fault ruptures and slip distributions of the Mw 6.6 11 April 2011 Hamadoori, Fukushima, northeast Japan, earthquake. *Bull. Seism. Soc. Am.* in press.

Murotani, S., Miyake, H. and Koketsu, K. (2008). Scaling of characterized slip models for plate-boundary earthquakes. *Earth Planets Space.* **60,** 987-991.

Shiba, Y. and Irikura, K. (2005). Rupture process by waveform inversion using simulated annealing and simulation of broadband ground motions. *Earth Planets Space.* **57,** 571-590.

Shiba, Y., Higashi, S., Sato, H., Sato, K. and Narita, A. (2009). Rock-outcrop Strong-motion (Kyoshin) observation network system (RK-net): Its development and application, *Japan Geoscience Union Meeting*, S222-P004.

Shiba, Y. and Noguchi, S. (2012). Statistical characteristics of seismic source parameters controlling broadband strong ground motions -Investigation based on source inversion analysis-. *CRIEPI REPORT.* **N11054** (in Japanese with English abstract).

Shiba, Y., Noguchi, S., Sato, H., Kuriyama, M. and Higashi, S. (2012). Source process of the 2011 M 9.0 off the Pacific coast of Tohoku earthquake by inversion analysis using strong-motion records. *CRIEPI REPORT.* **N11058** (in Japanese with English abstract).

Si, H. and Midorikawa, S. (1999). New attenuation relationships for peak ground acceleration and velocity considering effects of fault type and site condition. *J. Struct. Constr. Eng.* **523**, 63-70 (in Japanese with English abstract).

Somerville, P., Irikura, K., Graves, R., Sawada, S., Wald, D., Abrahamson, N., Iwasaki, Y., Kagawa, T., Smith, N. and Kowada, A. (1999). Characterizing crustal earthquake slip models for the prediction of strong ground motion. *Seism. Res. Lett.* **70,** 59-80.

Wessel, P. and Smith, W. H. F. (1998). New, improved version of Generic Mapping Tools released. *Eos Trans. Am. Geophys. Union.* **79**, 579.

Wu, C., Koketsu, K. and Miyake, H. (2008). Source processes of the 1978 and 2005 Miyagi-oki, Japan, earthquakes: Repeated rupture of asperities over successive large earthquakes. *J. Geophys. Res.* **113**, B08316, doi: 10.1029/2007JB005189.

Yagi, Y. and Fukahata, Y. (2011). Rupture process of the 2011 Tohoku-oki earthquake and absolute elastic strain release. *Geophys. Res. Lett.* **38,** L19307, doi:10.1029/2011GL048701.